ARTICLE   OPEN

First-principles-based prediction of yield strength in the RhIrPdPtNiCu high-entropy alloy

Binglun Yin[1] and William A. Curtin[1]

High-entropy alloys are random alloys with five or more components, often near equi-composition, that often exhibit excellent mechanical properties. Guiding the design of new materials across the wide composition space requires an ability to compute necessary underlying material parameters via ab initio methods. Here, density functional theory is used to compute the elemental misfit volumes, alloy lattice constant, elastic constants, and stable stacking fault energy in the fcc noble metal RhIrPdPtNiCu. These properties are then used in a recent theory for the temperature and strain-rate dependent yield strength. The parameter-free prediction of 583 MPa is in excellent agreement with the measured value of 527 MPa. This quantitative connection between alloy composition and yield strength, without any experimental input, motivates this general density functional theory-based methodological path for exploring new potential high-strength high-entropy alloys, in this and other alloy classes, with the chemical accuracy of first-principles methods.

INTRODUCTION

High-entropy alloys (HEAs), also called multiple principal element alloys, nominally consist of five or more elements at near-equal compositions in a single crystalline phase.[1] Many HEAs possess high yield strengths, ultimate strengths, and/or ductility, making them a broad new class of candidates for structural applications.[2–4] As a result, new materials are emerging rapidly. In the noble metal family, Sohn et al.[5] reported a single-fcc-phase RhIrPdPtNiCu system with compressive yield strength $\sigma_y = 527$ MPa, ultimate strength of 1839 MPa, and strain to failure of 32.4%, the latter two properties rivaling the strongest and toughest steels.[6] However, HEAs must not only match currently available structural alloys but exceed them in one or more properties. Since there is no physical restriction to near-equi-composition random alloys, the available composition space for multi-property optimization is vast. Searching through that space can be greatly facilitated by theory and modeling for both property prediction and phase stability. Accurate predictions require both accurate theories and the chemically accurate inputs to those models, and the latter leads to the application of first-principles methods.

Strength and ductility depend on the motion and interaction of dislocations through the random alloy. First-principles modeling of dislocations in pure elemental metals alone is challenging. Studying the required properties/behaviors of dislocations in complex HEAs is even more formidable. Thus, theories are needed to predict the desired properties based on computationally accessible material inputs. The first property of interest is the initial yield strength. This is the stress at which pre-existing dislocations can first start to move through the crystalline lattice and generate the on-going plastic strain at the macroscopic imposed strain-rate and temperature. A general theory has been developed to predict the temperature and strain-rate dependent yield strength in random fcc alloys.[7,8] The theory envisions the

HEA as an "effective-medium matrix", and each elemental atom in the alloy acts as a solute in the effective matrix. With an additional assumption that the solute/dislocation interaction energies are governed by elasticity, the model then requires only the average material properties of the alloy matrix and the properties of the elemental solutes in that average matrix.

Here, we use first-principles density functional theory (DFT) to compute all the necessary alloy properties that enter the theory, for the 6-component RhIrPdPtNiCu alloy studied recently. We present a new and general method to compute the required solute misfit volumes in the multicomponent random alloys, which then enables parameter-free and experiment-free prediction of the yield strength. Good agreement with experiment is achieved, establishing the overall methodology as a framework for computationally guided design of new fcc HEAs.

RESULTS

Theory of yield strength in multicomponent random alloys

We consider a general fcc alloy containing N_{elem} types of alloying elements at concentrations $\{c_n\}$ (with $\sum_{n=1}^{N_{elem}} c_n = 1$), with all alloying elements distributed randomly on the fcc lattice sites. There is thus a probability c_n that any given lattice site will be occupied by a type-n atom. The strengthening of the random alloy arises through solute/dislocation interactions. The interaction of the dislocation with the random fluctuations in the local solute concentrations induces the dislocation to become wavy over some characteristic wavelength $4\zeta_c$ and amplitude w_c that minimize the total energy of the system. The wavy dislocation is then locally trapped in low-energy regions. Dislocation motion, and plastic strain, thus occurs by stress-assisted thermal activation across the adjacent high-energy regions along the dislocation glide plane and into the next low-energy regions. The theory

computes the fundamental zero-stress energy barrier ΔE_b and zero-temperature flow stress τ_{y0} from which the yield stress at finite temperature T and finite strain-rate $\dot{\epsilon}$ are obtained. The theory is well described in the recent literature[8] and has been validated against molecular dynamics simulations in model alloys using semi-empirical interatomic potentials.[7]

To make the theory computationally accessible, it has been simplified through the use of elasticity theory.[7] In this limit, the solute/dislocation interaction energy of a type-n solute in the alloy is modeled as $-p(x, y)\Delta V_n$ where $p(x, y)$ is the elastic pressure field at solute position (x, y) due to a dislocation centered at the origin and ΔV_n is the average misfit volume of the type-n solute in the alloy. With this simplification, the theory becomes analytic for fcc alloys. Specifically, the zero-stress activation barrier ΔE_b and the zero-temperature shear yield stress τ_{y0} (stress at which the energy barrier is zero) are

$$\Delta E_b = 2.5785 \left[\frac{\Gamma}{b^2}\right]^{\frac{1}{3}} b^3 P^{\frac{2}{3}} \delta^{\frac{2}{3}},$$

$$\tau_{y0} = 0.04865 \left[\frac{\Gamma}{b^2}\right]^{-\frac{1}{3}} P^{\frac{4}{3}} \delta^{\frac{4}{3}},$$

(1)

where b is the dislocation Burgers vector, and

$$\delta = \sqrt{2 \sum_n c_n \Delta V_n^2 / (9b^6)}$$

(2)

is the well-known δ-parameter that describes the collective effect of the misfit volumes of all the elements in the alloy. In addition,

$$\Gamma = \alpha \mu_{110/111} b^2,$$
$$\mu_{110/111} = (C_{11} - C_{12} + C_{44})/3$$

(3)

are the dislocation line tension and shear modulus for fcc slip on the {111} plane in the $\langle 110 \rangle$ direction expressed in terms of the standard cubic elastic constants, respectively. The dimensionless line tension parameter $\alpha = 1/8$ is accurate for several fcc metals. The last quantity in Eq. (1) is an elastic coefficient $P = P(C_{ij})$ associated with the anisotropic dislocation pressure field. For fcc metals, P can be written in terms of appropriate averaged isotropic elastic constants μ^{ave} and ν^{ave} as

$$P(C_{11}, C_{12}, C_{44}) = \mu^{ave} \frac{1 + \nu^{ave}}{1 - \nu^{ave}}.$$

(4)

Previous applications of the model used experimentally measured isotropic elastic constants of the alloy, μ^{expt} and ν^{expt}.[7,9,10] A forthcoming full anisotropic analysis will demonstrate that the use of the Voigt-averaged elastic constants

$$\mu^V = (C_{11} - C_{12} + 3C_{44})/5,$$
$$\nu^V = \frac{3B - 2\mu^V}{2(3B + \mu^V)},$$
$$B = (C_{11} + 2C_{12})/3,$$

(5)

where B is the bulk modulus agrees with the full anisotropic model to within ~3% over a wide range of elastic anisotropy. We will thus use the Voigt-averaged values.

The resulting strength versus temperature T and strain-rate $\dot{\epsilon}$ is

$$\tau_y(T, \dot{\epsilon}) = \tau_{y0}(T) \left[1 - \left(\frac{k_B T}{\Delta E_b(T)} \ln \frac{\dot{\epsilon}_0}{\dot{\epsilon}} \right)^{\frac{2}{3}} \right],$$

(6)

where $\dot{\epsilon}_0 = 10^4 \, \mathrm{s}^{-1}$ is a reference strain-rate determined by the dislocation density and other factors. The properties entering $\tau_{y0}(T)$ and $\Delta E_b(T)$ should in principle be computed at the temperature of interest, especially the elastic constants. We discuss this further in Section "Yield strength prediction." Experiments are typically performed in uniaxial tension on random untextured polycrystalline specimens. The measured uniaxial yield

stress is related to the shear yield stress as $\sigma_y = M\tau_y$ where $M = 3.06$ is the Taylor factor for random fcc polycrystals.

Dislocations in fcc metals dissociate into two partial dislocations separated by a stacking fault. The two partials are separated by a distance d and each partial dislocation also spreads across a few atoms with the spreading characterized by a Gaussian function with standard deviation σ. This complex dislocation structure should thus influence the strengthening, since the solutes interact with the actual dislocation structure. Full analysis of the elastic theory as a function of d reveals that the strength is nearly *independent* of d for $d \gtrsim 6.5b$. The spreading parameter σ has been examined in several atomistic simulations using interatomic potentials and the typical values are $1.5 \leq \sigma/b \leq 2.0$. The analytic model above (Eq. (1)) with the numerical coefficients given corresponds to a sufficiently large partial separation $d \gtrsim 6.5b$ and $\sigma/b = 1.5$. The use of these values has yielded very good predictions in comparison with experiments.[7,9,10]

From the above summary, we see that the required inputs to the analytic theory are the fcc lattice constant (a_0 with $b = a_0/\sqrt{2}$), the elastic constants (C_{11}, C_{12}, C_{44}), and the solute misfit volumes (ΔV_n) at the alloy composition $\{c_n\}$. The partial separation must also be $d \gtrsim 6.5b$, which can be well-estimated in anisotropic elasticity as $d = K/\gamma_{ssf}$ where γ_{ssf} is the stable stacking fault energy of the alloy and K is an anisotropic elastic parameter computed exactly in terms of dislocation character, elastic constants, and Burgers vector.[11–15] All of the above quantities can be computed by first-principles using the methods described in Section "DFT methodology", leading to yield strength predictions given in Section "Yield strength prediction."

Misfit volumes

We consider, in general, an alloy containing N_{elem} types of alloying elements at concentrations $\{c_n\}$. The average misfit volume of a type-n atom in the random alloy can be conceptually defined as

$$\Delta V_n = \sum_m c_m \left\langle \Delta V^{n/m} \right\rangle,$$

(7)

where $\left\langle \Delta V^{n/m} \right\rangle$ is the volume change caused by replacing one type-m atom with type-n atom and with the brackets indicating averaging over many different such replacements where the atom of interest has different surrounding atomic environments.[16] Performing this actual procedure is computationally costly and unnecessary, but the definition remains useful. Operationally, we consider a macroscopic sample with N^{tot} atoms and total volume V_0^{tot} at the alloy composition. We then add ΔN_n type-n atoms by replacing $\Delta N_m = -\Delta N_n c_m/(1 - c_n)$ type-m atoms for all $m \neq n$ at randomly chosen type-m atom sites in the sample. The volume of the new random alloy is $V^{tot} = V_0^{tot} + \sum_m (-\Delta N_m) \langle \Delta V^{n/m} \rangle$. The average atomic volume $V = V^{tot}/N^{tot}$ can then be expressed as

$$V = V_0 + \Delta V_n x_s,$$
$$\text{with } x_s = \frac{\Delta N_n}{N^{tot}(1 - c_n)}.$$

(8)

After adding the additional type-n atoms, the changes of the elemental compositions are $(1 - c_n)x_s$ for the type-n atom and $-c_m x_s$ for all the other element types $m \neq n$. The new alloy can thus be considered as a pseudo-binary alloy with a formula $[\text{type}-n \text{ atom}]_{x_s}[\text{matrix}\{c_n\}]_{1-x_s}$, where the matrix is the original alloy and the "solutes" are the extra type-n atoms introduced into the effective matrix. Similarly, ΔN_n type-n atoms can be removed ($\Delta N_n < 0$) with other atom types added as $\Delta N_m = -\Delta N_n c_m/(1 - c_n)$ for all $m \neq n$. The total volume is then $V^{tot} = V_0^{tot} + \sum_m \Delta N_m \langle \Delta V^{m/n} \rangle$, with $\langle \Delta V^{m/n} \rangle = -\langle \Delta V^{n/m} \rangle$. This procedure leads again to Eq. (8), but with x_s being negative. Therefore, measuring the sample volume at different values of $|x_s| \ll 1$ for all solute types enables the determination of the

Table 1. Compositions and supercell formulas used here to compute misfit volumes

x_s (at.%)	Formula	N_{tot}
5.6	$A_6(ABCDEF)_{17}$	108
4.2	$A_6(ABCDEF)_{23}$	144
0.0	$A_0(ABCDEF)_{18}$	108
0.0	$A_0(ABCDEF)_{24}$	144
−3.1	$A_{-4}(ABCDEF)_{22}$	128

desired misfit volumes ΔV_n for all solutes in the alloy at the composition of interest.

To compute the average atomic volumes $V(x_s)$ of the various pseudo-binary random alloys, and the lattice constant and elastic constants at the central composition, there are various methods, such as cluster expansion (CE) method,[17] small set of ordered structures (SSOS) method,[18] similar local atomic environment (SLAE) method,[19] etc. To date, the two most widely used methods are the special quasi-random structures (SQS)[20] and the coherent potential approximation (CPA).[21] The supercell method combined with the concept of SQS has the very important advantage that explicit local lattice distortions within the SQS supercell are possible. On the other hand, the CPA method can mimic the perfect chemical disorder within one primitive cell. In this work, we need to compute the atomic volumes, lattice constants, and elastic constants precisely, where the local lattice distortion should be explicitly considered. Previous literature has shown that the local lattice relaxation has a significant effect on the alloy properties, e.g., formation energy.[22] We also wish to assess accuracy of the computed quantities, which can be accomplished using multiple realizations and sizes of the SQS cells. The SQS method is strongly preferred for these reasons, and is used here.

Application of the above strategy to the equi-composition 6-component (ABCDEF) alloy such as RhIrPdPtNiCu alloy is achieved as follows. We start with a supercell $(ABCDEF)_{N_0}$ (total number of atoms $N_{tot} = 6N_0$). We then add $5N_1$ atoms of type A and remove other atom types equally, leading to the pseudo-binary composition $A_{6N_1}(ABCDEF)_{N_0-N_1}$ with $x_s = 6N_1/N_{tot}$. Similarly, removing $5N_1$ atoms of type A and adding the other elements equally leads to the pseudo-binary composition $A_{-6N_1}(ABCDEF)_{N_0+N_1}$ and $x_s = -6N_1/N_{tot}$. This is repeated for each individual atom type (B, C, …) in the alloy. In fact, there is no actual need to use the same supercell when adding/removing atoms; this is just the clearest way to understand the process. Then, the pseudo-binary formula becomes of particularly high value. In practice, only the quantities $6N_1$ and $N_0 - N_1$ (or $-6N_1$, $N_0 + N_1$) need to be integers. For example, in Table 1, the $x_s = -3.1$ at.% case is achieved using $N_1 = 2/3$ and $N_0 = 64/3$, corresponding to $-6N_1 = -4$, $N_0 + N_1 = 22$ with $N_{tot} = 128$. The pseudo-binary concept thus leads to considerable flexibility in the choice of supercell size for each individual composition.

The choice of the supercell composition formulas is flexible but a few guidelines are helpful. First, N_{tot} should be neither too large nor too small. A large value is computationally costly while a small value might be insufficient for achieving an SQS of high quality. According to the literature, good representations of chemical disorder can usually be achieved using approximately several tens of atoms.[22] Second, $|x_s|$ should be neither too large nor too small. If too large, the volume change might exceed the domain of linear changes around the central composition. If too small, the uncertainty due to the configurational randomness will greatly increase the uncertainty in the deduced misfit volumes. The supercells and formula units used here are shown in Table 1, and satisfy $100 < N_{tot} < 150$ and $0.03 < |x_s| < 0.06$.

For each composition, the SQSs are generated *independently* using the ATAT code.[23] For the 6-element alloys here, SQS generation at the necessary supercell sizes of $100 \sim 150$ atoms is computationally intensive.[18] Fortunately, the resulting structures can be used multiple times by switching the atom types. In addition, these SQSs can immediately provide candidate SQSs for other alloys having fewer components with compositions in multiples of 1/6, such as A_2BCDE, A_4B_2, etc. For a given 6-component SQS, there are many different possible SQS structures for alloys with fewer components. The best SQS from among the possibilities is easily determined by evaluating the SQS quality, e.g., the SQS error using available error estimates.[24] The present SQSs can therefore be easily used for studying new alloys without any further time-consuming searches for new SQSs. For this reason, we provide the exact SQSs used here (https://doi.org/10.24435/materialscloud:2018.0019/v1).

With the SQS construction as described above, the equilibrium atomic volumes are computed by minimizing the total energy versus volume with full relaxation of all ions and supercell shape. We perform calculations for multiple samples at the same and/or various x_s to improve the overall accuracy of the final misfit volumes. From the entire set of DFT-computed equilibrium atomic volumes, we then perform a linear regression with one constraint $\sum_n c_n \Delta V_n = 0$ to obtain the misfit volumes ΔV_n for all solutes and the atomic volume V_0 at the desired composition $\{c_n\}$. Figure 1 shows the computed atomic volumes versus compositions x_s for all alloys studied here around the RhIrPdPtNiCu composition. We obtain the lattice constant and misfit volumes shown in Table 2. Importantly, from the totality of the data computed, we can compute the 95% confidence intervals for the lattice constant (± 0.00017 Å) and misfit volumes (± 0.093 Å^3), respectively. The misfit quantity δ in the theory for yield strength is then computed as $\delta = 3.873\%$, as shown in Fig. 1 and summarized in Table 2, with 95% confidence interval within $\pm 0.2\%$.

Elastic constants

The elastic constants of the alloy are computed starting from the equilibrium states of the two SQS structures of the random RhIrPdPtNiCu alloy containing 108 and 144 atoms, respectively. These systems have small initial (Pulay) stresses σ_i^0 ($i = 1...6$) using the Reuss contracted notation. We use the well-established stress method.[25] Six linearly independent strain tensors are applied (non-zero components = 0.002) and the corresponding stress tensors are computed in DFT. The elastic constants are then computed from $\sigma_i - \sigma_i^0 = C_{ij}\epsilon_j$. In one least-squares fitting, we calculate all 21 C_{ij} components of $C_{ij,108}$ and $C_{ij,144}$ (in GPa). The elastic constants expressed in the standard 6×6 Voigt matrix notation for the two different SQS cells are

$$\begin{bmatrix} 286 & 176 & 176 & -4 & -2 & -3 \\ & 296 & 182 & -4 & 1 & -3 \\ & & 297 & -5 & 0 & -2 \\ & & & 111 & -2 & -2 \\ & \text{Sym} & & & 113 & -2 \\ & & & & & 113 \end{bmatrix}, \begin{bmatrix} 284 & 172 & 171 & -1 & -3 & -2 \\ & 288 & 176 & -1 & 0 & -1 \\ & & 286 & 0 & -2 & -1 \\ & & & 111 & -1 & 0 \\ & \text{Sym} & & & 110 & -2 \\ & & & & & 112 \end{bmatrix}.$$

The fcc-symmetry is broken in these small cells of random alloys. To obtain the fcc constants C_{ij}, we take the averages of all the fcc-symmetry-equivalent components over both structures. The remaining C_{ij} components are set to zero (the averages being negligible). The resulting values are $C_{11} = 289$ GPa, $C_{12} = 176$ GPa, and $C_{44} = 112$ GPa. Since each elastic constant is an average over six values, we can compute the 95% confidence interval, which results in $\sim \pm 2\%$ of the mean value. The bulk modulus $B = (C_{11} + 2C_{12})/3 = 214$ GPa obtained from the averaging is very close to the values of B computed from the energy versus volume for the two structures (215 and 214 GPa, respectively).
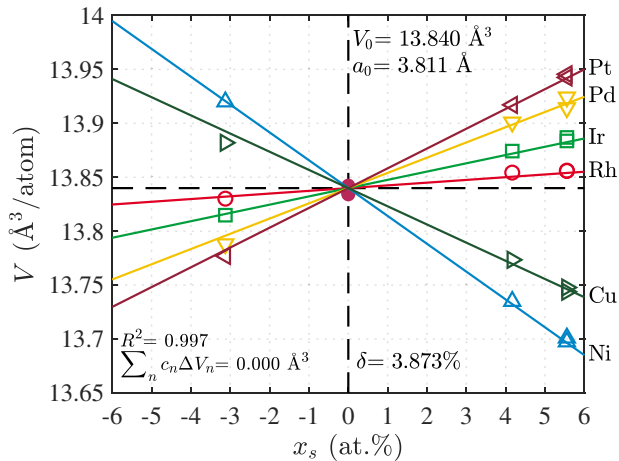
Fig. 1 Atomic volumes of random alloys at compositions surrounding the equi-composition RhIrPdPtNiCu alloy for various changes in composition. Solid lines show the linear regression that leads to the computed misfit volumes shown in Table 2, with the R^2 value indicated

Table 2. Lattice constant, misfit volumes, and δ-parameter from direct DFT calculations of the RhIrPdPtNiCu HEA

	Density functional theory (DFT)	Vegard's law
a_0 (Å)	3.811	3.800
ΔV_{Rh} (Å^3)	0.253	0.259
ΔV_{Ir} (Å^3)	0.767	0.799
ΔV_{Ni} (Å^3)	−2.581	−2.841
ΔV_{Pd} (Å^3)	1.412	1.605
ΔV_{Pt} (Å^3)	1.835	1.893
ΔV_{Cu} (Å^3)	−1.686	−1.715
δ (%)	3.873	4.193

Also show for comparison are results from the application of Vegard's law using the elemental DFT lattice constants

This alloy is moderately anisotropic, with Zener anisotropy index $A = 2C_{44}/(C_{11} − C_{12}) = 1.98$. The Voigt-averaged elastic constants that enter the strength theory are $\mu^V = 90$ GPa and $\nu^V = 0.316$. For this value of A, the full anisotropic value of P in Eq. (1) is only ~0.5% smaller than the isotropic approximation using these Voigt averages. The shear modulus used in the line tension is computed as $\mu_{110/111} = 75$ GPa.

Note that the *measured* shear modulus of the polycrystalline material is expected to be closer to the Voigt-Reuss-Hill average $\mu^{VRH} = 85$ GPa.[26] This value does not enter the strength theory and indicates the typical error that might be expected when using an experimentally measured shear modulus. All of the various elastic constants (anisotropic and associated isotropic average) for RhIrPdPtNiCu are shown in Table 3.

Stable stacking fault energy and partial separation

The stable stacking fault energy γ_{ssf} is computed using the ANNNI model. In this model, γ_{ssf} is related to the difference between hcp and fcc cohesive energies of the alloy as $\gamma_{ssf} = 2\left(E_0^{hcp} − E_0^{fcc}\right)/A_0^{fcc}$,

where E_0^{hcp} and E_0^{fcc} are the atomic energy for the fully relaxed hcp and fcc structures, respectively. A_0^{fcc} is the fcc atomic area on the stacking fault plane.

Table 3. Density functional theory (DFT)-computed material quantities at $T = 0$ K entering the solute strengthening model, and the resulting predicted yield strength at the experimental conditions of $T = 300$ K, $\dot{\epsilon} = 10^{-4}$ s^{-1}

a_0 (Å)	3.811		
δ (%)	3.873		
C_{11} (GPa) C_{12} (GPa) C_{44} (GPa)	289	176	112
μ^V (GPa) ν^V	90	0.316	
$\mu_{110/111}$ (GPa)	75		
σ_y (MPa)	583 (527)		

The experimentally reported yield strength is shown in parenthesis

Direct computation of γ_{ssf} in random alloys is deemed likely to have large fluctuations since it is a planar defect energy computed from two bulk energies of 3-dimensional random structures.[27] Furthermore, application of the analytic strengthening theory requires only that γ_{ssf} be sufficient to ensure sufficiently large partial dislocation separation d.

Benchmark DFT computations of γ_{ssf} for the individual elemental metals using the direct tilted-cell method[28] and ANNNI model show differences (which can be positive or negative) within ±20 mJ/m^2. The differences arise, in part, from the two fcc/hcp interfacial energies that are not considered in the ANNNI model.[29] We can thus anticipate that application of the ANNNI model to the 6-component alloy will have a similar level of uncertainty.

The formation energy of the fcc HEA phase is obtained from the previous DFT calcuations. For all fcc samples, we have the equilibrium energies. Performing a linear regression to the DFT energy data, analogous to what was done for the equilibrium atomic volumes in Fig. 1, gives the formation energy of fcc RhIrPdPtNiCu as $E_0^{fcc} = 34$ meV/atom, relative to the compositional average of the pure metal atomic energies in the fcc phase. The positive formation energy indicates that the single-phase RhIrPdPtNiCu HEA is either entropically stabilized or metastable. This result is in contrast to a negative formation energy roughly estimated from an empirical literature model.[5] To calculate E_0^{hcp}, we use the process employed for fcc at the composition of interest. We create the hcp SQSs for the HEA (https://doi.org/10.24435/materialscloud:2018.0019/v1), and perform DFT calculations to obtain the ground state energy on the compositions surrounding the central composition to improve the accuracy, and then perform linear regression to the DFT energy data for hcp structures. The resulting formation energy of RhIrPdPtNiCu in hcp phase is $E_0^{hcp} = 61$ meV/atom relative to the same compositional average of the pure metal atomic energies in the fcc phase. With $A_0^{fcc} = (\sqrt{3}/4)a_0^2$, the ANNNI model yields a stable stacking fault energy $\gamma_{ssf} = 138$ mJ/m^2 for RhIrPdPtNiCu. The uncertainty in γ_{ssf} is determined from the 95% confidence intervals of E_0^{fcc} and E_0^{hcp}, which are ±1 and ±2 meV, respectively. Therefore, the uncertainty in the DFT result itself for γ_{ssf} is about ±15 mJ/m^2. Combined with the intrinsic error/uncertainty of the ANNNI model, a conservative estimate of the uncertainty in the stable stacking fault energy is ~ ±35 mJ/m^2.

Finally, using the computed anisotropic elastic constants and lattice constant, the elastic parameter is $K = 0.180$ eV/Å and the estimated partial separation is then $d = K/\gamma_{ssf} = 7.8b$. Considering the uncertainty in γ_{ssf}, the corresponding partial separation ranges from $6.2b$ to $10.4b$. This estimation is an upper bound of the uncertainty since the value ±20 mJ/m^2 is probably higher than the true value in the HEA. The analysis thus generally satisfies the requirement $d \gtrsim 6.5b$ for applying the analytic solute strengthening model above.

Yield strength prediction

With all of the necessary material properties computed via DFT as described in the previous section, the yield strength of the alloy can be predicted. The experiments were performed at $T = 300$ K and strain-rate $\dot{\varepsilon} = 10^{-4}$ s^{-1}. As shown in Table 3, the predicted strength using only the DFT-computed inputs is $\sigma_y = 583$ MPa. The uncertainty in this prediction due to the uncertainties in DFT-computed materials parameters is small. Using the 95% confidence intervals of the lattice constant, misfit volumes, and elastic constants, the 95% confidence interval for the strength prediction is ~±10% of the above mean value. This uncertainty is due to the configurational randomness in the computations, at the SQSs qualities that we achieve.

The average prediction of 583 MPa is in very good agreement with the single experimental value of 527 MPa. While there is only one experimental data point, the yield strength of well-characterized alloys usually has small scatter. As analyzed in previous work using approximate methods,[10] this as-cast alloy has two different phases but these phases have very similar lattice constants and estimated strengths. The above experimental value is thus likely close to the "true value" of a single-phase homogenous alloy.

There are a few other aspects that could affect the strength prediction here. First, the DFT-calculated elastic constants must have some (unknown) error, as demonstrated by the deviations between DFT and experiment for the elemental metals. Here, we might expect that the Perdew-Burke-Ernzerhof (PBE) DFT predictions of the elastic moduli C_{ij} of the HEA are slightly lower than the (unknown) true experimental values due to the underestimate of the moduli of elemental Pd and Pt, as discussed in Section "DFT methodology."

Second, the experiments are at room temperature and so the room-temperature elastic constants should be used in the predictions. Room-temperature calculations are possible but computationally onerous, and so here we make reasonable estimates based on the elemental values. In experiments, the elastic constants C_{ij} of the pure metals all decrease, but by less than 10% from $T = 0$ K to $T = 300$ K. Therefore, the yield strength predictions made using the $T = 0$ K elastic constants are likely <10% too high. Thus, use of the (unknown) $T = 300$ K elastic constants would bring the predictions closer to the experimental value. For purposes of efficient identification of trends for alloy design, we advocate the use of the easily computed $T = 0$ K elastic constants, with temperature effects at room temperature estimated from a concentration-weighted average of the elemental elastic constants.

Third, the lattice constant a_0 and the δ-parameter are also temperature-dependent. Applying Vegard's law (defined below) using the temperature-dependent lattice constants of the pure metals to estimate both the alloy volume and solute misfit volumes at finite temperature, we find that the overall δ-parameter decreases by <2% with increasing temperature. The thermal expansion effects can thus be safely neglected.

Although there are uncertainties in the DFT-computed properties and the temperature dependencies, there are no adjustable/fitted parameters in the model. Overall, we thus consider the predictions to be robust and the agreement indicative of the applicability of the theory.

DISCUSSION

The present methodology can be expanded to scan over a wide range of the composition space so as to predict optimized composition(s) with the highest yield strength(s). Suppose we have a database of the atomic volumes over a set of equi-spaced compositions spanning the entire configurational space. Then one could fit the entire set to some overall function of the compositions, i.e., $V(\{c_n\})$. The misfit volume of type-n atom at composition $\{c_n\}$ could be computed by taking the derivative respect to x_s in the direction of $\{(1 - c_n)$ for n, $-c_m$ for $m \neq n\}$, i.e.,

$$\Delta V_n = \frac{V(\{c_n + (1 - c_n)x_s, c_m - c_m x_s\}) - V(\{c_n\})}{x_s}, \tag{9}$$

with $x_s \rightarrow 0$. Here, the challenging task is the computation of the data set. In order to have a quantitative estimate of the size of the database, we assume that the well-spaced compositions consist of elemental concentrations spanning from 0 to 100% by the step of 10%. For senary alloys studied here, the database needs 3003 different compositions for SQS sizes of ~100 atoms; this is not computationally feasible at present. However, for quaternary and ternary alloys, such a database requires 286 and 66 compositions, respectively, and so could be achieved computationally. In any case, the computation of the data set remains demanding but the methodology for the misfit volumes remains useful and will become more feasible as computational power increases.

Given the combinatoric challenge of performing DFT over the huge composition space of a many-component alloy, it is very useful to consider other more-approximate but more-efficient approaches. One such approach is by assuming Vegard's law and assuming a simple rule-of-mixtures for elastic constants.[10] Then only the lattice constants and elastic constants of the elemental metals are needed in the crystal structure of the HEA. These quantities are computationally trivial to obtain if all the elements are metastable in the HEA crystal structure. Vegard's law uses the atomic volumes $V_0^{(n)}$ of the individual elements and predicts the atomic volume of the alloy as $V_0^{\text{Vegard}} = \sum_n c_n V_0^{(n)}$. The misfit volumes follow as $\Delta V_n^{\text{Vegard}} = V_0^{(n)} - V_0^{\text{Vegard}}$. The rule-of-mixtures (ROM) estimate for the elastic constants is simply $C_{ij}^{\text{ROM}} = \sum_n c_n C_{ij}^{(n)}$ and yields a rule-of-mixtures Voigt average for the required μ and ν. With DFT results computed explicitly here for fcc RhIrPdPtNiCu, we can assess the accuracy of such a simple model since all the elements are stable in the fcc structure.

Using the DFT-computed atomic volumes for the constituents of the RhIrPdPtNiCu, Vegard's law yields $\delta = 4.193\%$. This is ~8% larger than the direct DFT result of $\delta = 3.873\%$ on the actual random alloy, as compared in Table 2. Similarly, using the DFT values for the elastic constants of the elements, the alloy ROM values are $C_{11}^{\text{ROM}} = 326$ GPa, $C_{12}^{\text{ROM}} = 177$ GPa and $C_{44}^{\text{ROM}} = 131$ GPa. Two of these values are ~15% larger than the DFT-computed alloy values (Table 3). The resulting Voigt estimate μ^V is then ~20% larger (108 GPa vs. 90 GPa). With the approximate estimates for both δ and μ^V being larger than the true DFT-computed properties for the alloy, the predicted strength using the approximate model is 775 MPa, which is rather larger than the full prediction.

The approximate approach above is thus of limited value for *quantitative* prediction in this family of alloys. However, the approximate approach may be too high mainly due to the moduli estimates, and the moduli estimates may be systematically high for other composition in the configurational space. This can be further validated with the calculations at other $\{c_n\}$.

The approximate approach may be useful only for rapid *relative* assessment of the relative strengths of alloy compositions. But even such a relative assessment can then point to a limited set of promising new alloy compositions that could be studied *quantitatively* using the computationally intensive but chemically accurate DFT calculations proposed in this work.

In summary, we have presented a general approach to DFT-level computations of the properties necessary to make strength predictions in HEAs and other random alloys using a recent analytic theory. The theory requires solute misfit volumes, alloy lattice constant, elastic constants, and stable stacking fault energy, all of which are accessible within current DFT capabilities. The DFT computational methodology for misfit volumes in

multicomponent random alloys is new and general. Executing the methodology on the fcc RhIrPdPtNiCu HEA, we obtain parameter-free predictions of the yield strength with no experimental inputs and find very good agreement with the experimental strength. We are also able to assess uncertainties in the approach and to assess concepts for highly efficient scanning of the huge composition space of HEAs. This work thus connects alloy composition to yield strength, establishing a general first-principles methodology for the computationally guided design of high-strength alloys.

METHODS

DFT methodology

All first-principles calculations are performed using DFT as implemented in the vasp code[30] within the generalized gradient approximation (GGA) and using the PBE XC functional.[31] The core electrons are replaced by the projector augmented wave (PAW) pseudopotentials.[32] The valence-electron eigenstates are expanded using a spin-polarized plane wave basis set with a cutoff energy 550 eV. A first-order Methfessel-Paxton method[33] with smearing parameter 0.2 eV is used. In reciprocal space, a Γ-centered Monkhorst-Pack[34] k-mesh is used with line density consistent across all geometries. The interval between the neighboring k-points along each reciprocal lattice vector $\mathbf{b}_j$ is 0.02 Å^{-1} (in vasp, $\mathbf{a}_i \cdot \mathbf{b}_j = \delta_{ij}$). This k-mesh density leads to, for example, $14 \times 14 \times 14$ for Ni and Cu in the fcc cubic unit cell, and $13 \times 13 \times 13$ for the other four elements. Ionic forces are relaxed to less than 1 meV/Å, corresponding to a stress tolerance of ~0.01 GPa in vasp. Benchmark calculations of the lattice constant, elastic constants, and stable stacking fault energy for the pure metal elements are in very good agreement with previous DFT literature.[35–37]

In the benchmark results for the elements, the PBE functional predicts the bulk moduli for Rh, Ir, Ni, and Cu within ±5% of experiment values but underestimates the bulk moduli of Pd and Pt by ~13% (169 GPa vs. 195 GPa for Pd, 249 GPa vs. 288 GPa for Pt; see ref.[35] (Table S25.3) and ref.[38]). Results using the PBEsol functional[39] improve the results for Pd and Pt relative to experiments but increase the differences between DFT and experiments for the other four elements in the alloy. These trends are already known in the literature. For this study, we use PBE so as to capture the better agreement with experiment for four of the six alloying elements studied here.

DATA AVAILABILITY

The data that support the findings of this study are available from the corresponding authors upon reasonable request. The SQSs used in this work are provided in (https://doi.org/10.24435/materialscloud:2018.0019/v1).

AUTHOR CONTRIBUTIONS

The initial project idea was from W.A.C., B.Y. and W.A.C. devised the methodology for the DFT computation of misfit volumes in multicomponent random alloys. B.Y. performed all the calculations. B.Y. and W.A.C. analyzed the results and wrote the manuscript.

ADDITIONAL INFORMATION

REFERENCES

1. Miracle, D. B. & Senkov, O. N. A critical review of high entropy alloys and related concepts. *Acta Mater.* **122**, 448–511 (2017).
2. Gludovatz, B. et al. A fracture-resistant high-entropy alloy for cryogenic applications. *Science* **345**, 1153–1158 (2014).
3. Miao, J. et al. The evolution of the deformation substructure in a Ni-Co-Cr equiatomic solid solution alloy. *Acta Mater.* **132**, 35–48 (2017).
4. Li, Z. & Raabe, D. Strong and ductile non-equiatomic high-entropy alloys: Design, processing, microstructure, and mechanical properties. *JOM* **69**, 2099–2106 (2017).
5. Sohn, S. et al. Noble metal high entropy alloys. *Scr. Mater.* **126**, 29–32 (2017).
6. Kimura, Y., Inoue, T., Yin, F. & Tsuzaki, K. Inverse temperature dependence of toughness in an ultrafine grain-structure steel. *Science* **320**, 1057–1060 (2008).
7. Varvenne, C., Luque, A. & Curtin, W. A. Theory of strengthening in fcc high entropy alloys. *Acta Mater.* **118**, 164–176 (2016).
8. Varvenne, C., Leyson, G. P. M., Ghazisaeidi, M. & Curtin, W. A. Solute strengthening in random alloys. *Acta Mater.* **124**, 660–683 (2017).
9. Varvenne, C. & Curtin, W. A. Strengthening of high entropy alloys by dilute solute additions: CoCrFeNiAlx and CoCrFeNiMnAlx alloys. *Scr. Mater.* **138**, 92–95 (2017).
10. Varvenne, C. & Curtin, W. A. Predicting yield strengths of noble metal high entropy alloys. *Scr. Mater.* **142**, 92–95 (2018).
11. Wu, Z., Yin, B. & Curtin, W. A. Energetics of dislocation transformations in hcp metals. *Acta Mater.* **119**, 203–217 (2016).
12. Anderson, P. M., Hirth, J. P. & Lothe, J. *Theory of dislocations* (Cambridge University Press, https://www.cambridge.org/ch/academic/subjects/engineering/materials-science/theory-dislocations-3rdedition?format=HB&isbn=9780521864367, 2017).
13. Ting, T. C. T. *Anisotropic elasticity: Theory and applications* (Oxford University Press, https://global.oup.com/academic/product/anisotropic-elasticity-9780195074475?q=Anisotropic%20Elasticity:%20Theory%20and%20Applications&lang=en&cc=ch, 1996).
14. Stroh, A. N. Dislocations and cracks in anisotropic elasticity. *Philos. Mag.* **3**, 625–646 (1958).
15. Bacon, D., Barnett, D. & Scattergood, R. Anisotropic continuum theory of lattice defects. *Prog. Mater. Sci.* **23**, 51–262 (1980).
16. Varvenne, C., Luque, A., Nöhring, W. G. & Curtin, W. A. Average-atom interatomic potential for random alloys. *Phys. Rev. B* **93**, 104201 (2016).
17. Sanchez, J. M., Ducastelle, F. & Gratias, D. Generalized cluster description of multicomponent systems. *Phys. A Stat. Mech. its Appl.* **128**, 334–350 (1984).
18. Jiang, C. & Uberuaga, B. P. Efficient Ab initio modeling of random multi-component alloys. *Phys. Rev. Lett.* **116**, 105501 (2016).
19. Song, H. et al. Local lattice distortion in high-entropy alloys. *Phys. Rev. Mater.* **1**, 023404 (2017).
20. Zunger, A., Wei, S. -H., Ferreira, L. G. & Bernard, J. E. Special quasirandom structures. *Phys. Rev. Lett.* **65**, 353–356 (1990).
21. Vitos, L., Abrikosov, I. A. & Johansson, B. Anisotropic lattice distortions in random alloys from first-principles theory. *Phys. Rev. Lett.* **87**, 156401 (2001).
22. Ikeda, Y., Grabowski, B. & Körmann, F. Ab initio phase stabilities and mechanical properties of multicomponent alloys: A comprehensive review for high entropy alloys and compositionally complex alloys. *Mater. Charact.* **147**, 464–511 (2019).
23. Van De Walle, A. et al. Efficient stochastic generation of special quasirandom structures. *Calphad Comput. Coupling Phase Diagr. Thermochem.* **42**, 13–18 (2013).
24. Von Pezold, J., Dick, A., Friák, M. & Neugebauer, J. Generation and performance of special quasirandom structures for studying the elastic properties of random alloys: Application to Al-Ti. *Phys. Rev. B* **81**, 094203 (2010).
25. Le Page, Y. & Saxe, P. Symmetry-general least-squares extraction of elastic data for strained materials from ab initio calculations of stress. *Phys. Rev. B* **65**, 104104 (2002).
26. Hill, R. The elastic behaviour of a crystalline aggregate. *Proc. Phys. Soc. Sect. A* **65**, 349–354 (1952).
27. Zhao, S., Stocks, G. M. & Zhang, Y. Stacking fault energies of face-centered cubic concentrated solid solution alloys. *Acta Mater.* **134**, 334–345 (2017).
28. Yin, B., Wu, Z. & Curtin, W. A. Comprehensive first-principles study of stable stacking faults in hcp metals. *Acta Mater.* **123**, 223–234 (2017).
29. Li, R. et al. Stacking fault energy of face-centered cubic metals: Thermodynamic and ab initio approaches. *J. Phys. Condens. Matter* **28**, 395001 (2016).
30. Kresse, G. & Furthmüller, J. Efficient iterative schemes for ab initio total-energy calculations using a plane-wave basis set. *Phys. Rev. B* **54**, 11169–11186 (1996).
31. Perdew, J. P., Burke, K. & Ernzerhof, M. Generalized gradient approximation made simple. *Phys. Rev. Lett.* **77**, 3865–3868 (1996).
32. Kresse, G. & Joubert, D. From ultrasoft pseudopotentials to the projector augmented-wave method. *Phys. Rev. B* **59**, 1758–1775 (1999).
33. Methfessel, M. & Paxton, A. T. High-precision sampling for Brillouin-zone integration in metals. *Phys. Rev. B* **40**, 3616–3621 (1989).
34. Monkhorst, H. J. & Pack, J. D. Special points for Brillouin-zone integrations. *Phys. Rev. B* **13**, 5188–5192 (1976).

35. Lejaeghere, K. et al. Reproducibility in density functional theory calculations of solids. *Science* **351**, aad3000 (2016).

36. Shang, S. L. et al. First-principles calculations of pure elements: Equations of state and elastic stiffness constants. *Comput. Mater. Sci.* **48**, 813–826 (2010).

37. Wu, X. Z., Wang, R., Wang, S. F. & Wei, Q. Y. Ab initio calculations of generalized-stacking-fault energy surfaces and surface energies for FCC metals. *Appl. Surf. Sci.* **256**, 6345–6349 (2010).

38. Simmons, G. & Wang, H. *Single Crystal Elastic Constants and Calculated Aggregate Properties: A Handbook* (The M.I.T. Press, https://mitpress.mit.edu/books/single-crystal-elastic-constants-and-calculated-aggregate-properties-secondedition, 1971).

39. Perdew, J. P. et al. Restoring the density-gradient expansion for exchange in solids and surfaces. *Phys. Rev. Lett.* **100**, 136406 (2008).